

Ammonia Decomposition in a Dielectric Barrier Discharge plasma: Insights from experiments and kinetic modeling

Supporting Information

J. A. Andersen^a, K van 't Veer^b, J. M. Christensen^a, M. Østberg^c, A. Bogaerts^b and A. D. Jensen^{a,*}.

^a *Department of Chemical and Biochemical Engineering, Technical University of Denmark, 2800 Kgs. Lyngby, Denmark*

^b *Research group PLASMANT, Department of Chemistry, University of Antwerp, 2610 Wilrijk, Belgium*

^c *Topsoe A/S, Haldor Topsøes Allé 1, 2800 Kgs. Lyngby, Denmark*

**Corresponding author: Aj@kt.dtu.dk (A.D. Jensen)*

1 Effect of feed flow rate, frequency, and plasmas power on N_{MD}

The number of micro-discharges per half cycle (N_{MD}) was determined for all the experiments shown in section 4.1 of the main text by assessing their case-specific power profile. Interestingly, the feed flow rate and the plasma power did not affect N_{MD} significantly (see Table S1). However, at lower frequencies (1.0 and 1.5 kHz) the N_{MD} was clearly higher than at the higher frequencies tested. Yet, on a time basis, the number of micro-discharges (per second) increased with frequency. The measured peak-to-peak voltage (V_{pk-pk}) show a decreasing trend as the flow rate and frequency are increased and an increasing trend when the plasma power is increased (Table S1). However, the current spike intensity is not significantly affected by the flow rate and only slightly lowered with lower plasma power and higher frequency.

Table S1. Effect of operational parameters on the number of micro-discharges per half cycle and measured peak-to-peak voltage.

Constant parameters			Constant parameters			Constant parameters		
Frequency [kHz]	3.0		Flow rate [Nml/min]	100		Frequency [kHz]	3.0	
Power [W]	15		Power [W]	15		Flow rate [Nml/min]	100	
Variable parameter			Variable parameter			Variable parameter		
Flow rate [Nml/min]	N_{MD}	V_{pk-pk} [kV]	Frequency [kHz]	N_{MD}	V_{pk-pk} [kV]	Power [W]	N_{MD}	V_{pk-pk} [kV]
50	7	23.5	1.0	16	32.6	10	6	20.6
75	8	23.1	1.5	11	27.3	12.5	7	21.3
100	9	22.7	2.0	8	24.8	15	9	22.7
125	7	22.4	2.5	8	23.4	17.5	8	23.3
			3.0	9	22.7	20	9	24.0
			3.5	7	22.2	22.5	9	24.2
						25	8	23.8

2 Model inputs

Several inputs were given to the model, as described in the computational method (section 3) in the main text, with many of them determined from our experiments, such as temperature, pressure, reactor volume, reduced electric field (E/N), the number of micro-discharges per half cycle (N_{MD}), and the lifetime of a single micro-discharge (τ_{MD}). Furthermore, the charge transfer (Q_0), burning voltage (ΔU), capacitance of the cell (C_{cell}), effective capacitance (ζ_{diel}), and dielectric capacitance (C_{diel}) (shown in Table S2, along with N_{MD} and τ_{MD}) are determined from the voltage and charge measurements by plotting these in a Q-U Lissajous diagram as described in our previous work (Andersen et al., 2022). These parameters are used to calculate the average plasma power (\bar{P} , Equation S1), when taking into account the partial discharging scenario described by Peeters and van de Sanden (Peeters and Sanden, 2015), where α (Equation S2) describes the non-discharging fraction and $\beta (= 1 - \alpha)$ the discharging fraction of the volume. A constant frequency (f_D) of 3.0 kHz was used in the experiments related to the kinetic modelling.

$$\bar{P} = 2U_b \Delta Q_D f_D = 2 \left(1 + \frac{\alpha C_{cell}}{\beta C_{diel}} \right) \Delta U \frac{Q_0}{1 - \frac{C_{cell}}{C_{diel}}} f_D \quad \text{Eq S1}$$

$$\alpha = \frac{C_{diel} - \zeta_{diel}}{C_{diel} - C_{cell}} \quad \text{Eq S2}$$

The average plasma power is then used to calculate the maximum instantaneous power (P_{max}):

$$P_{max} = \frac{\bar{P}}{(1 - \gamma) 2 N_{MD} f_D \tau_{MD} \xi_s + \gamma} \quad \text{Eq S3}$$

where γ is the power distribution factor and ξ_s is a pulse shape factor (van 't Veer et al., 2020) equal to $\frac{1}{2}$, giving a triangular power density pulse. The minimum instantaneous power (P_{min}) is determined from P_{max} :

$$P_{min} = \gamma P_{max} \quad \text{Eq S4}$$

The equivalent maximum and minimum power densities can then be determined from Equation S3 and S4, by defining the average power density as $\bar{p} = P/V$ (van 't Veer et al., 2020). The maximum and minimum power densities are then used to determine the periodic power density function ($p(t)$), as described

in van 't Veer et al. (2020). The electric field (E) is then evaluated from the power density and the electron conductivity (σ , Equations S5 and S6):

$$E = \sqrt{\frac{p(t)}{\sigma}} \quad \text{Eq S5}$$

$$\sigma = en_e\mu_e \quad \text{Eq S6}$$

where e is the elementary charge, n_e is the electron number density, and μ_e is the electron mobility, calculated by BOLSIG+.

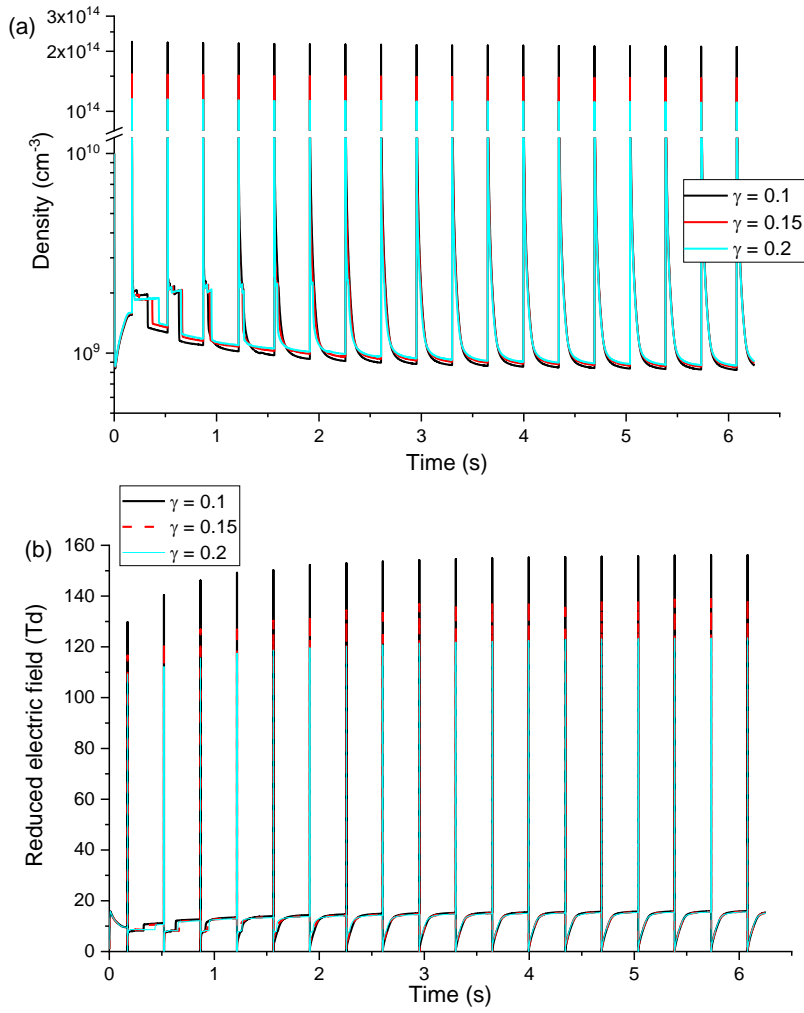
Table S2. Case-specific parameters used as input to the plasma kinetic model for calculating the power density.

	Discharge length [cm]	Q_0 [nC]	ΔU [V]	C_{cell} [pF]	ζ_{diel} [pF]	C_{diel} [pF]	N_{MD}	τ_{MD} [ns]
No packing	1	337.0	6050	4.581	27.64	34.66	8	200
No packing	2	459.8	5700	6.721	37.56	45.07	9	200
No packing	5	563.2	5750	8.251	64.91	90.47	9	200
No packing	10	444.4	5050	12.35	61.22	141.4	9	200
No packing	15	413.3	4900	16.46	74.73	175.1	9	200
Packed	5	294.8	6700	10.51	60.97	77.80	30	200

3 Model prediction of electron density, temperature and reduced electric field

The effect of the power distribution factor (γ) between the micro-discharges and the uniform plasma on the electron density, reduced electric field (E/N), and electron temperature (T_e) are shown in Figure S1 for the unpacked setup. Note that the reduced electric field is expressed in Td, where $1 \text{ Td} = 10^{-17} \text{ V}\cdot\text{cm}^2$. Typical values in the order of 100-150 Td are reached in the micro-discharges, and around 10 Td in the afterglow. The electron density reaches about 1×10^{14} - $2 \times 10^{14} \text{ cm}^{-3}$ in the micro-discharges and drops to ca. 10^9 cm^{-3} in the afterglows, while the electron temperature is about 60000-70000 K (or 5-6 eV) in the micro-discharges and 8000 K (or 0.7 eV) in the afterglows. It is seen that a lower γ value, corresponding to a

more non-uniform plasma (hence: more intense micro-discharges), yields a higher electron density, reduced electric field, and electron temperature during micro-discharges, while the values in the afterglow are almost independent (only the electron density is slightly higher with higher γ).



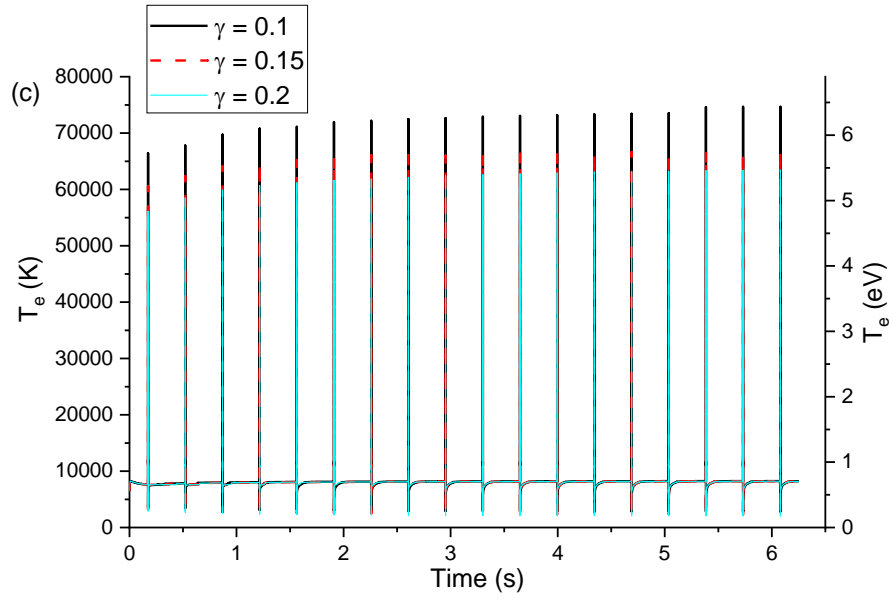


Figure S1. Effect of power distribution factor, γ , on the transient behaviour of (a) electron density, (b) reduced electric field, and (c) electron temperature, obtained for a residence time of 6.25 s.

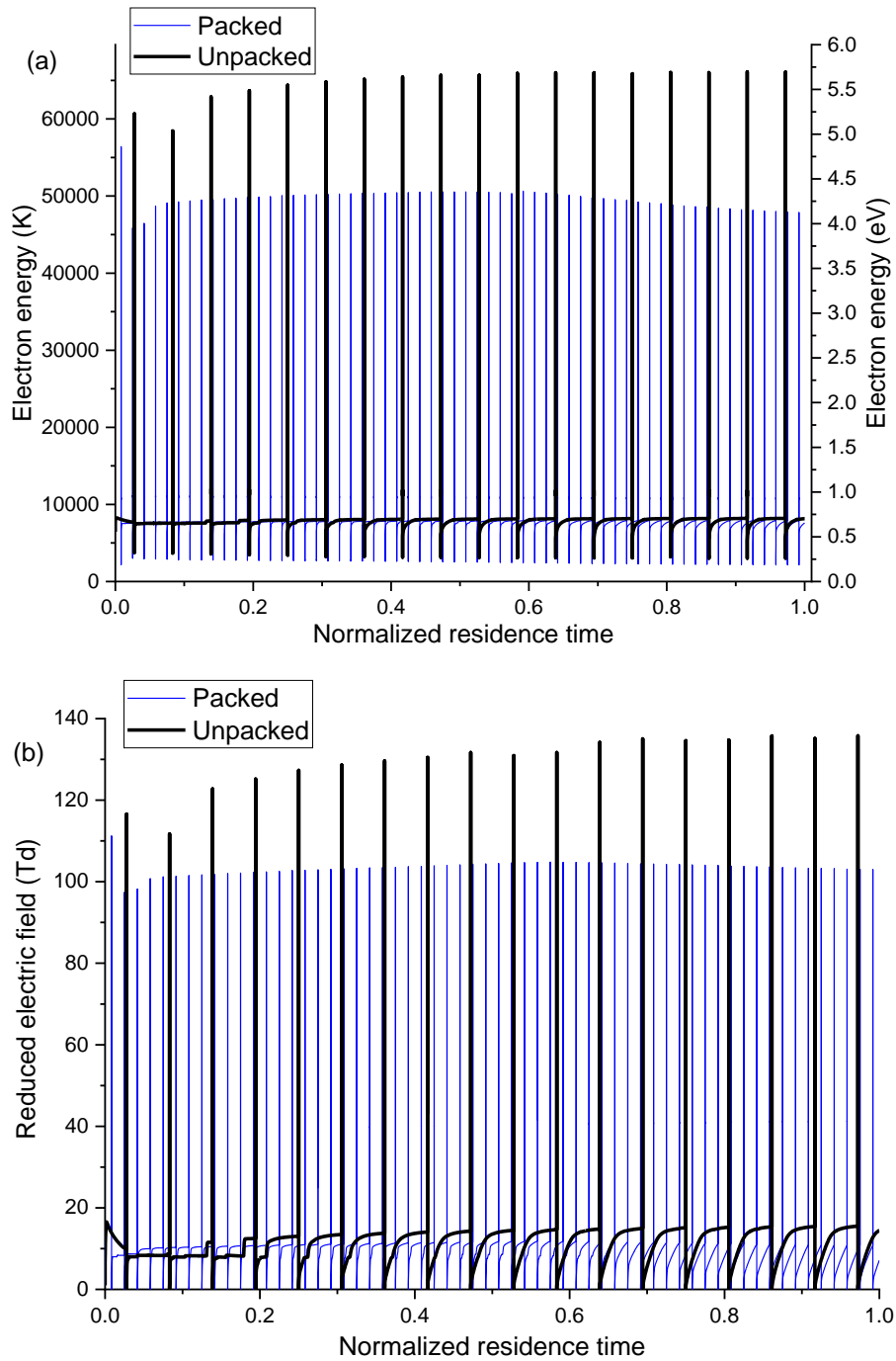


Figure S2. Comparison between (a) the average electron energy and (b) reduced electric field for the packed ($\gamma = 0.35$) and unpacked setup ($\gamma = 0.08$). The gas residence times have been normalized with respect to their corresponding full residence time.

The average electron energy for the packed and unpacked setup can be observed to sharply increase in the micro-discharges to values of 4-5 eV, followed by a steep decrease (Figure S2a). Quickly after the decrease, the value rises again during the afterglows to approximately 0.7 eV, which is similar for all the recorded afterglows, but the average electron energy for the packed setup is slightly lower. Furthermore, it is observed that the electron energy never drops to a value near zero. This is because a small power is transferred to the uniform plasma component in the afterglows (see detailed description in the main text and in van 't Veer et al. (2020)). A larger number of peaks are also seen in Figure S2a for the packed setup, which is due to the larger number of micro-discharges formed with packing material (see Table S2), but the values reached during the micro-discharges are lower than for the unpacked setup. This correlates with the higher γ found for the packed setup, making the power distribution more uniform (hence: less intense micro-discharges, see Figure S4). The reduced electric field for the packed and unpacked setup are shown in Figure S2b where values in the order of 95-110 and 110-140 Td are reached in the micro-discharges for the packed and unpacked setup, respectively. In the afterglows, the reduced electric field reaches values around 10 Td for the packed setup and slightly higher values for the unpacked. The lower electron energy and lower reduced electric field for the packed setup matches the observations seen in Figure S1, where a lower γ value yields a higher electron temperature and reduced electric field during micro-discharges ($\gamma = 0.35$ for packed and $\gamma = 0.08$ for unpacked setup). Furthermore, the measured peak-to-peak voltage was lower for the packed setup ($V_{pk-pk}=21.7$) compared to the unpacked ($V_{pk-pk}=26.3$).

Figure S3 shows the cumulated density of electrons for the packed and unpacked setup. There is a small increase during the afterglows (not observable on the figure) due to the constant power present in this phase (Figure S2), while stepwise increments are observed in the micro-discharges. Furthermore, the larger number of micro-discharges formed with packing material (Table S2), where the electron density is high, yields an increased number of steps. However, the increment in the steps is smaller for the

packed setup compared to the unpacked, which is consistent with the predicted electron density present in the micro-discharges, as described in the main text (cf. Figure 6).

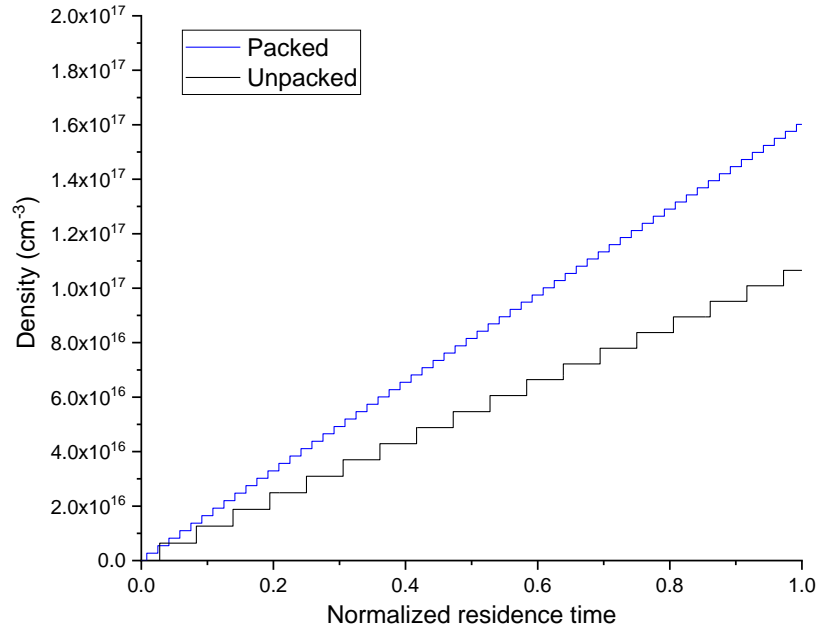


Figure S3. Cumulated electron density as a function of normalized residence time, for the packed ($\gamma = 0.35$) and unpacked setup ($\gamma = 0.08$).

The I-V characteristic for the plasma-only and with MgAl_2O_4 introduced in the plasma are shown in Figure S4. A large difference in the intensity of the current spikes can be observed when comparing the characteristics of the two systems. This means that the power deposited in the plasma trough micro-discharges is lower when having MgAl_2O_4 present in the plasma compared to the plasma-only. Correlating this to the plasma kinetic model shows that a higher γ is needed for the packed case to mimic the power distribution between micro-discharges and uniform plasma. As mentioned in the main text, $\gamma = 1$ corresponds to a fully uniform plasma, hence, according to the model, the packed system forms a more uniform plasma.

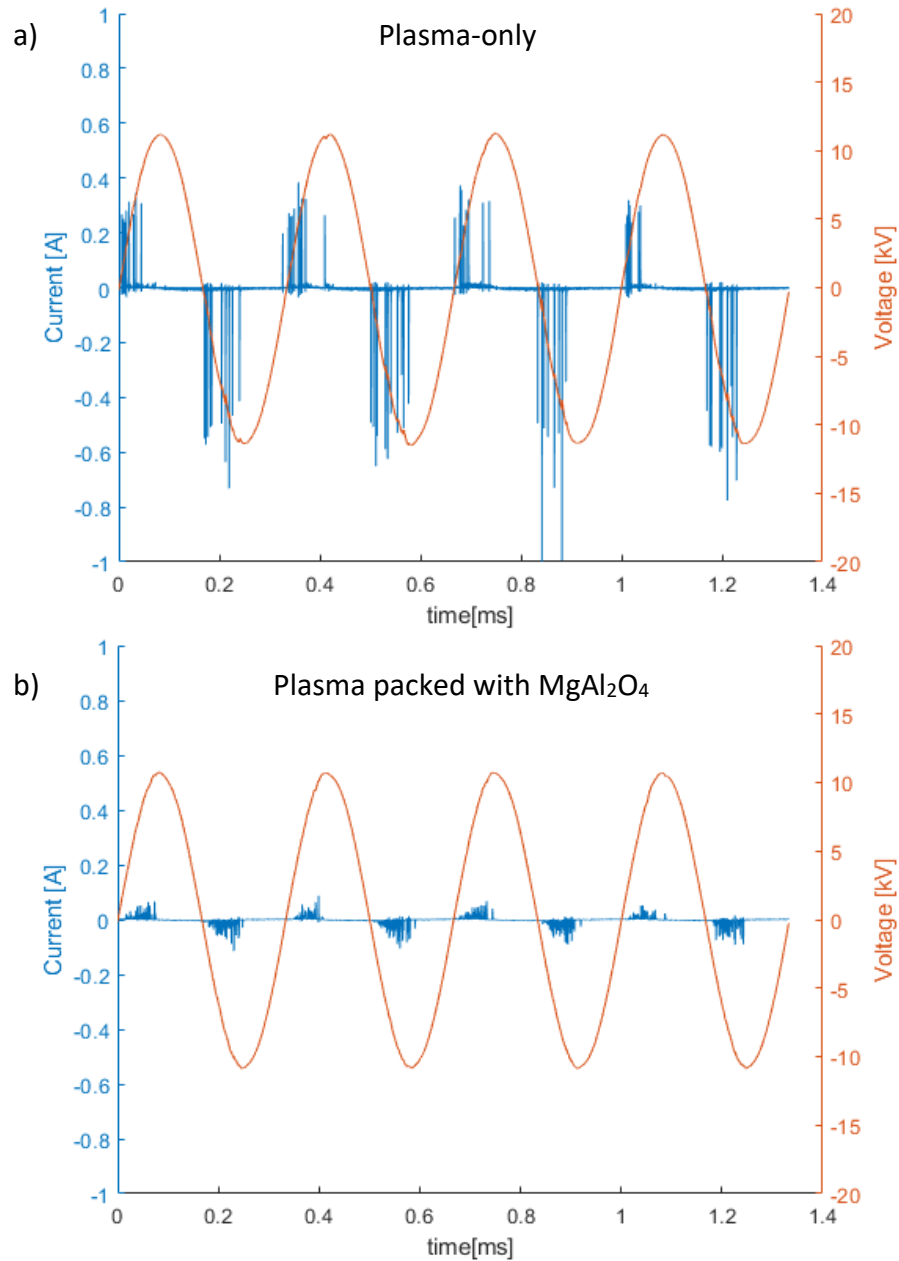


Figure S4. I-V characteristic for (a) plasma-only and (b) with MgAl_2O_4 in the plasma zone. Measurements obtained with a plasma power of 15 W and frequency of 3 kHz, flow rate of 100 Nml/min, and discharge gap of 4.5 mm.

4 Full transient development of plasma species density and surface coverage

Figure S5 and Figure S6 show the transient development of the species densities described in the main text over the full residence time for the unpacked and packed setup, respectively. For both setups, it is

found that the density of NH_3 decreases, while the N, N_2 , H, and H_2 densities increase, as expected from the decomposition. The relative increase in N_2 density is small due to the high N_2 content in the feed. Additionally, as an effect of the decreasing NH_3 density, the densities of NH_2 and NH slowly decrease. The density of NH_4^+ is found to be affected to a large extent by the micro-discharges, with relatively large changes in density between micro-discharge and afterglow.

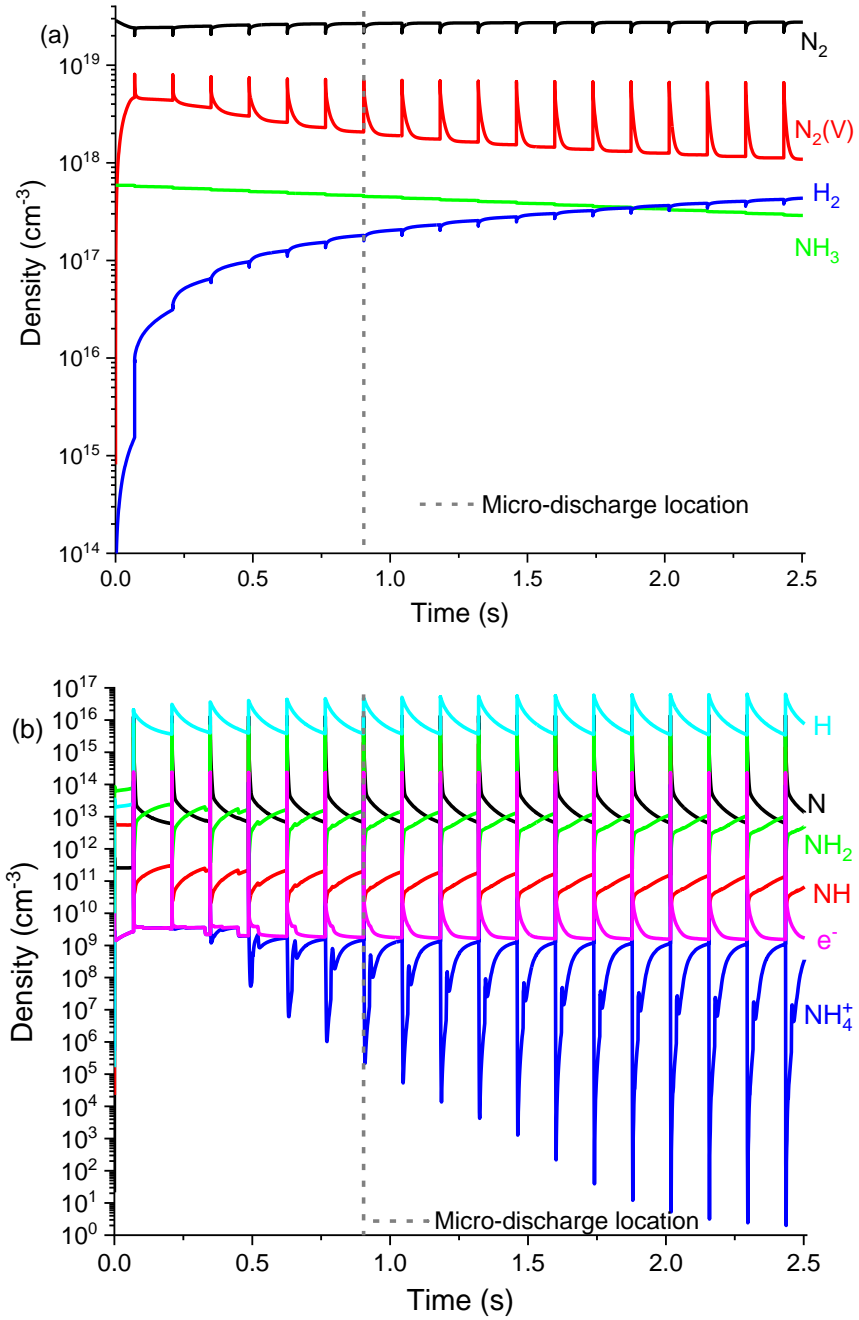


Figure S5. Full transient behavior of the number density of (a) neutral and vibrationally excited species and (b) radicals and charged species in the gas phase, obtained for unpacked setup with an outer electrode length of 2 cm and $\gamma = 0.08$.

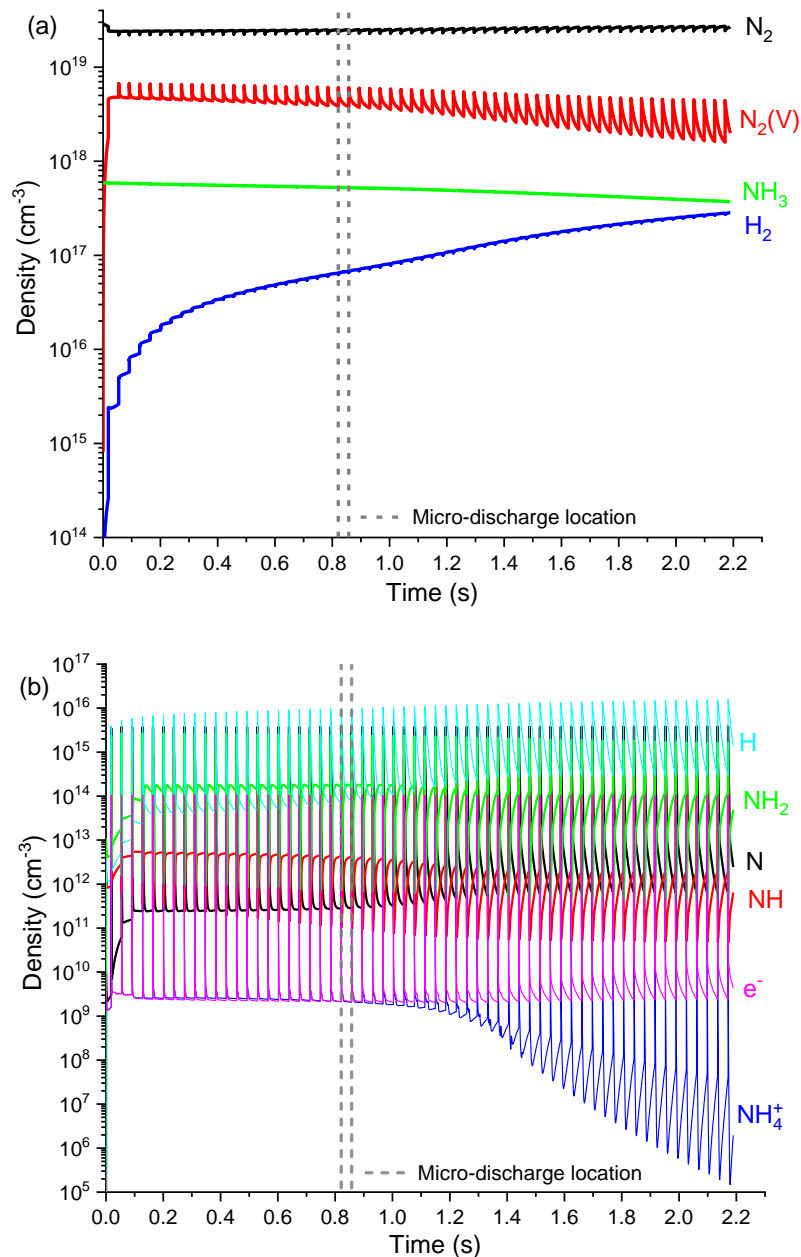


Figure S6. Full transient behavior of the number density of (a) neutral and vibrationally excited species and (b) radicals and charged species in the gas phase, obtained for packed setup with an outer electrode length of 5 cm and $\gamma = 0.35$.

The full transient development of the surface coverages are shown in Figure S7. The H(s) coverage is initially found to increase rapidly due to the formation of H in the gas phase, and as a consequence the N(s) coverage is decreasing. Moreover, the NH₂(s) and NH(s) coverages decrease as well, partly due to the

decrease in the densities of these species in the gas phase and the increasing coverage of H(s). The formation of NH₂(s) is also affected by the NH(s) coverage, as described in the main text, hence this is the reason for the general lower coverage of NH₂(s), even though the density of NH₂ is higher in the gas phase.

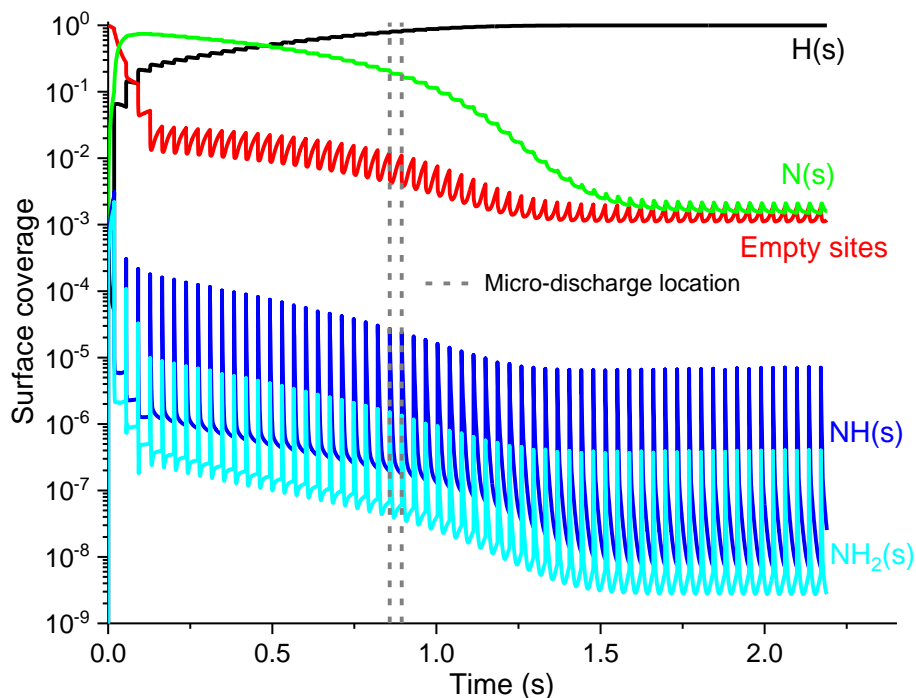


Figure S7. Full transient behavior of surface coverage and fraction of empty sites when operating with packing material with an outer electrode length of 5 cm and $\gamma = 0.35$.

5 Schematic reaction pathways for the packed setup

Figure S8 shows the reaction pathway for NH₃ decomposition for the packed setup, which is similar to the one presented in the main text for the unpacked setup and a description of this is given in section 4.6 of the main text. However, with the packing material present, the model determined different contributions of the individual reactions compared to the unpacked setup (Figure 9). Furthermore, an additional reaction in the afterglows was found by the model to contribute negatively to the NH₃ decomposition, with packing material present, i.e., Reaction 26 (indicated in red in Figure S7). Here, NH₂ reacts with surface-

bound hydrogen (H(s)) in an Eley-Rideal reaction to form NH₃. The introduction of more surface sites thereby has a negative effect on the overall NH₃ decomposition, as described in the main text.

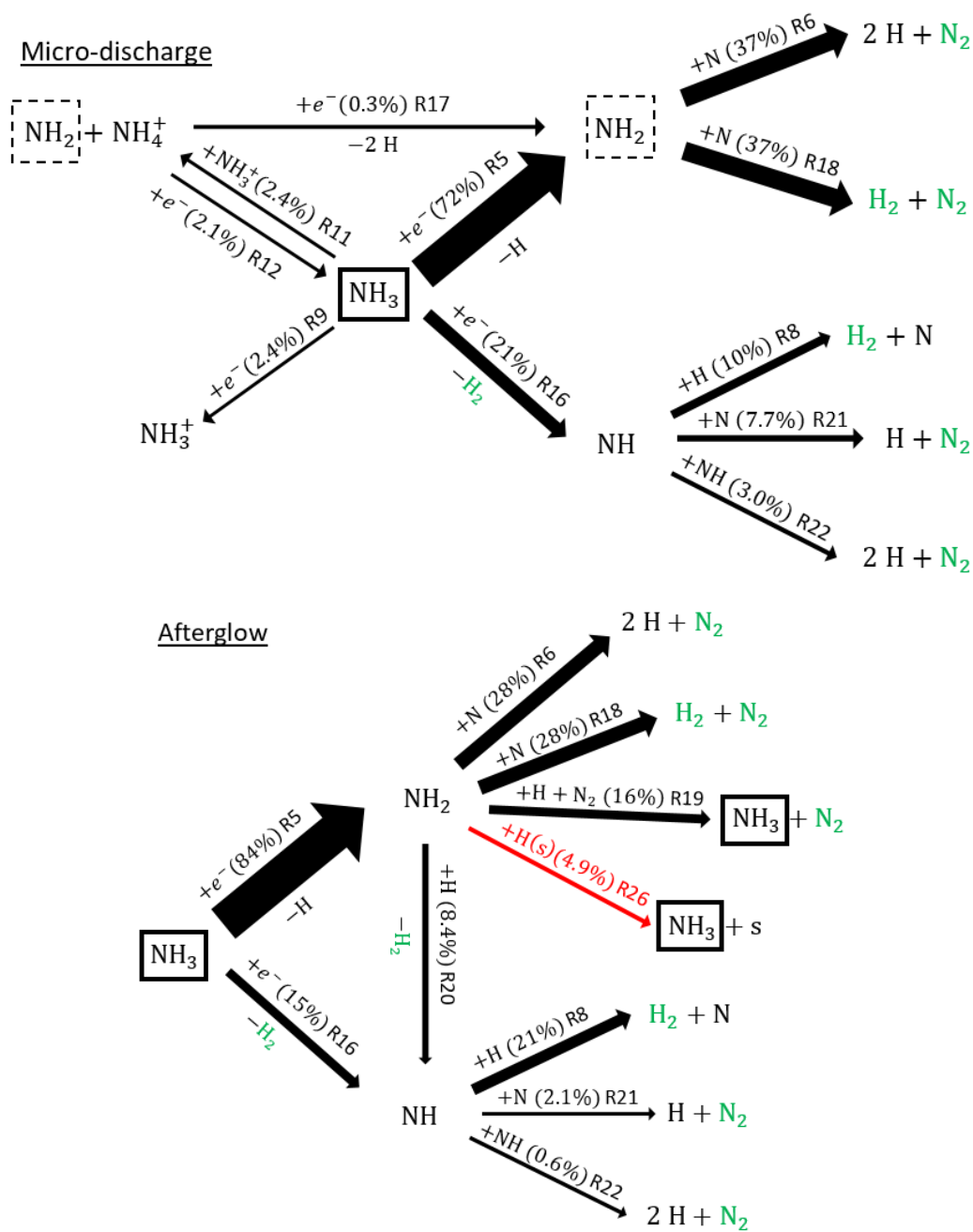


Figure S8. Schematic reaction pathways for NH₃ decomposition into H₂ and N₂ in a micro-discharge and its afterglow for a packed setup.

References

- Andersen, J.A., Christensen, J.M., Østberg, M., Bogaerts, A., Jensen, A.D., 2022. Plasma-catalytic ammonia decomposition using a packed-bed dielectric barrier discharge reactor. *Int. J. Hydrogen Energy*. <https://doi.org/10.1016/j.ijhydene.2022.07.102>
- Peeters, F.J.J., Sanden, M.C.M. van de, 2015. The influence of partial surface discharging on the electrical characterization of DBDs. *Plasma Sources Sci. Technol.* 24, 015016. <https://doi.org/10.1088/0963-0252/24/1/015016>
- van 't Veer, K., Reniers, F., Bogaerts, A., 2020. Zero-dimensional modelling of unpacked and packed bed dielectric barrier discharges: The role of vibrational kinetics in ammonia synthesis. *Plasma Sources Sci. Technol.* 29, 45020. <https://doi.org/10.1088/1361-6595/ab7a8a>